Paleoceanography and Paleoclimatology

RESEARCH ARTICLE
10.1029/2019PA003791

A Late Miocene to Late Pleistocene Reconstruction of Precipitation Isotopes and Climate From Hydrated Volcanic Glass Shards and Biomarkers in Central Alaska and Yukon

Gerard A. Otiniano[1], Trevor J. Porter[1], Jeff A. Benowitz[2], Ilya N. Bindeman[3], Duane G. Froese[4], Britta J. L. Jensen[4], Lauren J. Davies[4], and Michael A. Phillips[5]

[1]Department of Geography, University of Toronto – Mississauga, Mississauga, Ontario, Canada, [2]Geophysical Institute, University of Alaska, Fairbanks, Fairbanks, Alaska, USA, [3]Department of Earth Sciences, University of Oregon, Eugene, OR, USA, [4]Earth and Atmospheric Sciences, University of Alberta, Edmonton, Alberta, Canada, [5]Department of Biology, University of Toronto – Mississauga, Mississauga, Ontario, Canada

Abstract The Pliocene (5.3–2.6 Ma), an epoch with periods of climatic warmth and possible analogue for the future, has been well-characterized globally by marine geochemical proxies. However, far less is known about Pliocene warmth at continental high latitudes, where the greatest impacts of warming are expected. This study seeks to better characterize the Pliocene climate of central Alaska and Yukon based on a reconstruction of the stable hydrogen isotope composition of precipitation relative to modern ($\Delta\delta D_{precip}$) preserved in volcanic glass shards, a proxy for mean air temperature. The studied tephras are from a regional suite of outcrops that, when assembled into a composite record of $\Delta\delta D_{precip}$, can be used to resolve broad trends during the late Miocene (6.7–5.86 Ma, $n = 5$), Pliocene (5.08–2.81 Ma, $n = 7$), and late Pleistocene (0.74–0.03 Ma, $n = 3$). These trends indicate that Pliocene $\Delta\delta D_{precip}$ estimates were generally more enriched in heavy isotopes than the latest Miocene, Pleistocene, and modern intervals. $\Delta\delta D_{precip}$ is likely influenced by changes in regional boundary conditions including orographic barriers, depositional environments, and ocean-atmospheric circulation, but $\Delta\delta D_{precip}$ trends are most consistent with reconstructed temperatures from Yukon-Alaska and North Pacific marine records. As such, this record appears predominantly sensitive to regional climate. Furthermore, qualitative temperature inferences from branched-chain glycerol dialkyl glycerol tetraethers (brGDGTs) from four of our sites dating between 2.91 and 6.17 Ma corroborate elevated temperatures during the early Pliocene. Overall, this study demonstrates the viability of volcanic glass δD as a proxy for $\Delta\delta D_{precip}$ and late Cenozoic climate change in this region.

Key Points:
- The $^2H/^1H$ of hydrated volcanic glass shards in late Cenozoic ash beds in Yukon and Alaska document changes in meteoric $^2H/^1H$ ratios
- The $^2H/^1H$ glass record is most coherent with other terrestrial and marine temperature reconstructions, indicating strong climate sensitivity
- Branched-chain glycerol dialkyl glycerol tetraether (brGDGT) biomarkers from some of the same deposits corroborate significantly elevated temperatures during the early Pliocene

Supporting Information:
- Supporting Information S1
- Table S1

Correspondence to:
T. J. Porter,
trevor.porter@utoronto.ca

Citation:
Otiniano, G. A., Porter, T. J., Benowitz, J. A., Bindeman, I. N., Froese, D. G., Jensen, B. J. L., et al. (2020). A late Miocene to late Pleistocene reconstruction of precipitation isotopes and climate from hydrated volcanic glass shards and biomarkers in Central Alaska and Yukon. *Paleoceanography and Paleoclimatology*, *35*, e2019PA003791. https://doi.org/10.1029/2019PA003791

Received 15 OCT 2019
Accepted 25 APR 2020
Accepted article online 3 MAY 2020

Author Contributions:
Conceptualization: Gerard A. Otiniano, Trevor J. Porter
Data curation: Gerard A. Otiniano, Trevor J. Porter
Formal analysis: Gerard A. Otiniano
Funding acquisition: Gerard A. Otiniano, Trevor J. Porter, Jeff A. Benowitz
Investigation: Gerard A. Otiniano, Trevor J. Porter, Jeff A. Benowitz
(continued)

1. Introduction

Combustion of fossil fuels since industrialization has increased atmospheric carbon dioxide concentrations (pCO_2) which have, in turn, increased global mean surface temperatures (e.g., Hansen et al., 2013). This warming is being amplified in Arctic and sub-Arctic regions, partly due to positive climate-albedo feedbacks resulting from reduced sea ice and terrestrial snow cover and the northward migration of shrubs and trees into tundra areas (Berner et al., 2005; Serreze & Barry, 2011). It is expected that the average temperatures in these sensitive regions will continue to rise in the near term as the climate system equilibrates to the current pCO_2 levels (~410 ppm; Keeling et al., 2001) and in response to future emissions (Hansen et al., 2013). Although the direction of climate change in the Arctic is a near certainty, predicting the magnitude of future warming in high latitude regions is the subject of large uncertainties due to challenges in modeling all relevant processes in the Arctic climate system. Alternatively, natural climate proxy data in the geologic record of past periods, when pCO_2 was similar to or higher than today, can provide insight into what a future, warmer Arctic could look like.

One possible climate analogue is the Pliocene epoch (5.3 to 2.6 Ma), a period defined by similar-to-modern land–ocean boundary conditions and variable pCO_2 ranging from 250 to 450 ppm (Haywood et al., 2016). The Pliocene climate history of the global oceans is relatively well known based on a suite of organic and isotope geochemical indicators from marine sediment cores (Herbert et al., 2016; Zachos et al., 2001).

Methodology: Gerard A. Otiniano, Trevor J. Porter, Jeff A. Benowitz, Ilya N. Bindeman, Duane G. Froese, Britta J. L. Jensen, Lauren J. Davies, Michael A. Phillips
Resources: Trevor J. Porter, Jeff A. Benowitz, Ilya N. Bindeman, Duane G. Froese, Britta J. L. Jensen, Lauren J. Davies, Michael A. Phillips
Supervision: Trevor J. Porter
Validation: Gerard A. Otiniano, Trevor J. Porter, Jeff A. Benowitz, Ilya N. Bindeman, Duane G. Froese, Britta J. L. Jensen, Lauren J. Davies, Michael A. Phillips
Visualization: Gerard A. Otiniano
Writing - original draft: Gerard A. Otiniano, Trevor J. Porter, Michael A. Phillips
Writing – review & editing: Gerard A. Otiniano, Trevor J. Porter, Jeff A. Benowitz, Ilya N. Bindeman, Duane G. Froese, Britta J. L. Jensen, Lauren J. Davies, Michael A. Phillips

Conversely, Pliocene climate reconstructions from terrestrial high-latitude regions are scarce and often limited to discrete, coarsely dated intervals of time such as the late Pliocene (e.g., Csank, Patterson et al., 2011; Pound et al., 2015) or late Miocene/early Pliocene (e.g., Ager et al., 1994; Leopold & Liu, 1994). In central Yukon and Alaska, the area of interest, Miocene and Pliocene climate estimates are mostly based on fossil beetle (e.g., Elias & Matthews, 2002) or pollen (e.g., Leopold & Liu, 1994; Pound et al., 2015; White et al., 1997) assemblages. Moreover, different proxy types from the same site and stratigraphic unit do not always lead to consistent paleoclimate estimates. As such, further replication and independent proxies are needed to develop a clearer picture of this region's Pliocene climate history, with potential implications for better understanding the potential climate scenarios of the future. To this end, we present an ~7 Myr record of stable hydrogen isotope ratios of precipitation (δD_{precip}). δD_{precip} values are reconstructed from the isotopic composition of hydrated volcanic glass shards (δD_{glass}) from a suite of radiometrically dated tephras.

δD_{precip} is sensitive to changes in temperature and elevation (Dansgaard, 1964). Variations in δD_{precip} can be imprinted on the δD of organic and inorganic matrices preserved in the geologic record, for example, relict ice in permafrost (Porter et al., 2016, 2019), fossil hydrocarbons (Feakins et al., 2019; Thomas et al., 2018), or hydrated volcanic glass shards in tephra (Colwyn et al., 2019; Friedman et al., 1992, 1993; Friedman, Gleason, & Warden, 1993; Martin et al., 2017; Mulch et al., 2008). This study utilizes the δD of hydrated volcanic glass shards, a proxy for δD_{precip}, from tephra beds found throughout Alaska and Yukon, sourced from volcanoes in the St. Elias-Wrangell Mountains, Alaska Range, and the Aleutian Arc (Benowitz et al., 2007; Jensen et al., 2008; Preece et al., 2011; Reyes et al., 2010; Triplehorn et al., 1999; Wahrhaftig et al., 1969; Westgate et al., 2009). Due to limited Quaternary glaciation in central Alaska and north-central Yukon, these volcanic ash beds have remained largely undisturbed (Froese et al., 2009; Preece et al., 2011; Westgate et al., 1990).

Initially, ash deposits contain glass shards with very low magmatic (primary) water content (0.1–0.6 wt% H_2O (Friedman, Gleason, & Warden, 1993; Seligman et al., 2016; Taylor et al., 1983). However, volcanic glass may become hydrated over long periods of time (10^3–10^4 years) if deposited in settings which expose the ash to free environmental waters (referred to as secondary waters), such as precipitation (Friedman, Gleason, & Warden, 1993; Martin et al., 2017; Seligman et al., 2016). Glass hydration is initially a simple process of secondary water addition as can be demonstrated by comparing major and trace element chemistry of variably hydrated ash particles and perlites (Anovitz et al., 2009; Bindeman & Lowenstern, 2016; Friedman et al., 1966). Once fully hydrated, glass remains stable at constant near-surface conditions and is resistant to further degradation (Anovitz et al., 2009; Friedman, Gleason, & Warden, 1993). Degradation involves processes such as hydrolysis and dissolution, which alter glass geochemistry. For example, glass cations are exchanged for water-derived H^+, a process which is kinetically restricted and limited by diffusion and is further accompanied by precipitation and growth of new secondary minerals (Cerling et al., 1985; Gin et al., 2015; Parruzot et al., 2015). The concentration of water (primary and secondary) within glass shards with a depositional age more than ~2,000 years can be variable and range from <1 to 4–6 wt% H_2O (e.g., Dettinger & Quade, 2015; Martin et al., 2017; Mulch et al., 2008; Seligman et al., 2016). The lower range of H_2O concentrations is likely due to incomplete hydration of an initially anhydrous or water poor glass, whereas concentrations in excess of 10 wt% are likely due to the presence of secondary water-rich phases such as zeolites. This variability within 2–6 wt% (Friedman & Long, 1976) can be attributed to geochemical variations between glass shards (e.g., low silica vs high silica rhyolites) that influence not only the rates of hydration, but also water saturation. Similarly, because diffusion is a kinetic process, temperature may influence diffusion rates and therefore hydration, although this relationship is not yet fully understood. Moreover, there may also be more complicated kinetic processes which accelerate water diffusion (e.g., water concentration gradient across the glass surface) or decelerate diffusion (e.g., formation of a protective silica-rich "gel" layer on the shard surface; Anoviz et al., 2009; Gin et al., 2015; Parruzot et al., 2015; Seligman et al., 2016 Cassel & Breecker, 2017).

Previous studies have used δD of hydrated volcanic glass shards from Cenozoic tephras as a proxy for change in climate, depositional environment, and/or paleo-elevation, which influence δD_{precip} and the δD of secondary hydration waters (Bill et al., 2018; Canavan et al., 2014; Cassel et al., 2014, 2009, 2018; Cassel & Breecker, 2017; Dettinger & Quade, 2015; Friedman et al., 1992; Mix & Chamberlain, 2014; Mulch et al., 2008; Pingel et al., 2014, 2020). Here, we present the first composite Late Miocene to Late Pleistocene

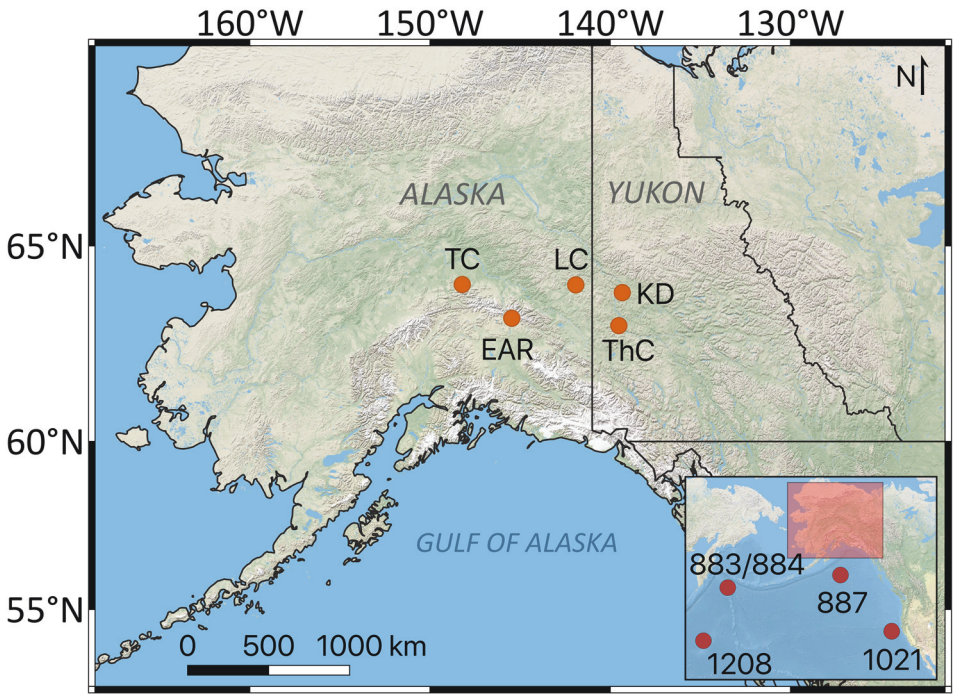

Figure 1. Locations of main study areas/localities in Alaska and Yukon including the following: Tanlanika Creek locality (TC); the Eastern Alaska Range (EAR) study area, which includes the Phelan Creek, McCallum Creek, Proposal Creek, and Lower and Upper Gunn Creek localities; the Lost Chicken Mine locality (LC); the Klondike (KD) study area, which includes the Goldbottom Creek and Quartz Creek localities; and Thistle Creek locality (ThC). The inset map shows the broader regional context including Ocean Drilling Program Sites 883/884, 887, 1021, and 1208.

reconstruction of δD_{precip} from a suite of tephras in continental Yukon-Alaska (Figure 1; Table 1). In the study region, δD_{precip} is strongly influenced by mean air temperature (Porter et al., 2016, 2019; Supporting Information) as well as factors such as atmospheric circulation and mean elevation, which makes attributing isotopic signals to any one factor difficult. As such, we interpret these data in the context of available previously published constraints on tectonics and paleotemperature from terrestrial proxy data (fossil pollen, insects, and leaf physiognomy) and North Pacific Sea Surface Temperature (SST) proxies. Additionally, we supplement the existing paleoclimate constraints with novel qualitative temperature inferences from bacterial branched-chain glycerol dialkyl glycerol tetraethers (brGDGTs) preserved in some of the same deposits as the studied tephras. These records of δD_{precip} (glass) and brGDGT proxies show robust, albeit coarsely resolved, patterns of variability over the last 6.7 Myr related to tectonics, Pliocene warmth, and Pleistocene cooling. Further, application of these proxies to deeper Cenozoic strata in southern Alaska holds great promise for better understanding the evolution of paleoenvironmental conditions following the onset of orogeny since ~30 Ma (Benowitz et al., 2019, 2014; Brueseke et al., 2019).

2. Materials and Methods

Tephras reported in this study are well known from previous studies and range between 6.70–0.03 Ma (Table 1). Tephra samples have been obtained from five localities in Alaska and Yukon: the Klondike (KD) and Thistle Creek (ThC) in central Yukon, the Lost Chicken Mine (LC) in eastern central Alaska, the windward slope of the Eastern Alaska Range (EAR), and the Tanlanika Creek (TC) on the lee slope of the Alaska Range (Figure 1). More information on the stratigraphic and geochronological context of the samples can be found in the supporting information and/or in Table 1.

2.1. Sample Collection and Preparation

Glass separates of the KD, ThC, and TC sites were obtained from the University of Alberta and tephrochronology collection and bulk materials from the LC and EAR sites were collected in the field, during the summer of 2017. Additionally, sediments associated with the tephras from Lost Chicken, Phelan Creek, Proposal

Paleoceanography and Paleoclimatology

10.1029/2019PA003791

Table 1

δD_{glass} and H_2O wt% Measurements and $\Delta\delta D_{precip}$ Estimates For Geochemically Unique Volcanic Glasses

Lab ID	Tephra name (locality, study area)	Lat., Long. (°, WGS84)	Site/ Tephra #	Age ± 1σ (Ma)	δD_{glass} ±1σ (‰)	$\Delta\delta D_{precip}$ ±1σ (‰)	H_2O ± 1σ (wt.%)	Depositional environment	Modern δD_{precip} ± 1σ (‰)	δD_{SW} ± 1σ (‰)
UA1005[*]	Dawson tephra (Goldbottom Creek, KD)	64.043, −139.42	1	0.0294 ± 0.0002[a]	−219 ± 3	−20 ± 3	2.39 ± 0.06	L	−164 ± 2	−10
UA1122 UT1774[†]	Old Crow tephra (Thistle Creek, ThC)	63.061, −139.522	2	0.12 ± 0.10[b]	−223 ± 7	−27 ± 7	3.91 ± 0.03	L	−158 ± 1	−14
UA1001	Gold Run tephra (Dominion Creek, KD)	63.691, −138.605	3	0.74 ± 0.06[c]	−223 ± 4	−16 ± 4	3.45 ± 0.03	L	−162 ± 2	−23 ± 3
UA1004	Quartz Creek tephra (Quartz Creek, KD)	63.816, −139.058	4	2.81 ± 0.34[§]	−201 ± 3	−4 ± 3	3.13 ± 0.03	CM	−161 ± 2	−10 ± 2
UA2947 UA2945	Lost Chicken tephra (Lost Chicken Mine, LC)	64.053, −141.871	5	2.91 ± 0.44[d]	−177 ± 8	24 ± 8	5.96 ± 0.02	ORM	−161 ± 2	−13 ± 2
UA2988	Wai tuff (Phelan Creek, EAR)	63.205, −145.546	6	3.81 ± 0.05[e]	−196 ± 2	4 ± 3	6.16 ± 0.02	LORM	−165 ± 2	−9 ± 1
UA2976	unnamed tephra (McCallum Creek, EAR)	63.231, −145.632	7	4.63 ± 0.05[e]	−200 ± 3	−2 ± 3	4.94 ± 0.02	FC	−165 ± 2	−6 ± 2
UA2977	unnamed tephra (Proposal Creek, EAR)	63.219, −145.439	8.1	5.08 ± 0.06[e]	−199 ± 3	−6 ± 4	5.19 ± 0.02	LORM	−158 ± 3	−9 ± 2
UA2987	unnamed tephra (Proposal Creek, EAR)	63.219, −145.439	8.2	5.08 ± 0.06[e]	−181 ± 3	12 ± 4	5.01 ± 0.05	LORM	−158 ± 3	−9 ± 2
UA2989	unnamed tephra (Proposal Creek, EAR)	63.219, −145.439	8.3	5.08 ± 0.06[e]	−164 ± 3	30 ± 4	5.10 ± 0.02	LORM	−158 ± 3	−9 ± 2
UA2975	unnamed tephra (Lower Gunn Creek, EAR)	63.207, −145.360	9	5.86 ± 0.19[e]	−218 ± 3	−23 ± 3	5.28 ± 0.05	LFS	−160 ± 3	−10 ± 2
UA2973	unnamed tephra (Upper Gunn Creek, EAR)	63.207, −145.401	10.1	6.17 ± 0.07[e]	−205 ± 3	−9 ± 3	4.95 ± 0.05	LFSs	−161 ± 4	−10 ± 2
UA2972	unnamed tephra (Upper Gunn Creek, EAR)	63.207, −145.401	10.2	6.17 ± 0.07[e]	−215 ± 3	−19 ± 3	4.97 ± 0.05	LFS	−161 ± 4	−10 ± 2
UA2974	unnamed tephra (Upper Gunn Creek, EAR)	63.207, −145.401	10.3	6.17± 0.07[e]	−210 ± 3	−13 ± 3	5.4 ± 0.02	LFS	−161 ± 4	−10 ± 2
UA2240	Grubstake tephra (Tanlanika Creek, TC)	64.078, −148.210	11	6.70 ± 0.08[f]	−182 ± 2	20 ± 2	4.92 ± 0.01	FBP	−160 ± 2	−10 ± 1

Note. Where replicates of the same glasses were collected (e.g., Lost Chicken tephra and Old Crow tephra), the δD_{glass}, H_2O wt%, and $\Delta\delta D_{precip}$ values given in this table represent the mean of all replicates. Lab ID is the lab number for each tephra in the University of Alberta tephra geochemistry database. For outcrops with more than one tephra bed (i.e., Proposal Creek and Gunn Creek), stratigraphic position is indicated by the decimal of the site/tephra # (e.g., "x.1" is the lowest [oldest] position). The depositional environment of each tephra is denoted as follows: loess (L), organic rich mudstones (ORM), colluvial material above fluvial sands (CM), fluvial conglomerates (FC), lacustrine organic rich mudstones (LORM), lacustrine fine-grained sands (LFS), and a forest bed associated with a paleosol (FBP).

[a]Froese et al. (2006). [b]Preece et al. (2011). [c]Westgate et al. (2009). [d]Matthews et al. (2003). [e]Allen (2016). [f]Triplehorn et al. (1999). [†] Two separate samples of the Old Crow tephra from Thistle Creek were analysed; the results of each analysis are available in Table S1. [§]The Quartz Creek tephra age given here represents the average of two dating methods, $^{40}Ar/^{39}Ar$ (Kunk, 1995) and weighted fission track (Westgate et al., 2002). Additionally, the age of this tephra is further constrained to the gauss interval, C2An.1n sub-chron (2.581 to 3.032 Ma). [*]A δD_{glass} value of −241.5 ± 3‰ was previously reported for UA1005 (Dawson tephra) by Porter et al. (2016). The δD_{glass} value of −219 ± 1.82‰ reported here is based on the same UA1005 raw δD data generated by Porter et al. (2016), but accounts for a revision to the nominal values of the internal silicate calibration standards included in the original analysis.

Creek, and Gunn Creek (with the exception of Lower Gunn Creek) were collected for brGDGT analysis. At each outcrop, colluvium and the outer 30–40 cm of sediment-containing surface weathered tephra was removed prior to sampling. Approximately 500 grams per tephra or sediment sample was hand-collected and stored in Whirl-Pak bags. After outcrop cleaning and sample collection, glass separates were extracted following standard procedures (Jensen et al., 2008). Samples were wet sieved into 149–74 μm and 74–44 μm fractions and washed with 10% HCl and 3% H_2O_2 to remove adherent carbonate and organic material, respectively. To further disaggregate mineral assemblages and clean the glass, the samples were sonicated for 75 min in an ultrasonic bath. The glass shards were then isolated using heavy liquid separation ($\rho = 2.40 \pm 0.05$ g/ml). The glass samples were examined optically under cross-polarized light to confirm high purity.

2.2. Major and Minor Element Analysis

To distinguish multiple tephras from each site and to evaluate their correlation with reference materials in the University of Alberta tephrochronology database, we measured major and minor elemental composition from the 149–74 μm glass fraction using a JOEL 8900R Superprobe (at 6 nA, 15 keV, and 5–10 μm ion beam) at the University of Alberta. Some samples were analyzed using a 5-μm beam and time-dependent intensity correction to account for Na loss using the Probe for EPMA software (Donovan et al., 2015). For quality control, the Lipari obsidian (ID3506) and Old Crow tephra were analyzed multiple times during the analytical session. Elemental compositions were normalized to 100% and are presented in the supplementary information.

2.3. δD_{glass} Measurements

Samples of the 74–44 μm glass fraction were vacuum dried for 48 hours at 250°C and then analyzed for glass δD (δD_{glass}) composition at the Stable Isotope Laboratory at the University of Oregon. δD_{glass} values were quantified using a temperature conversion elemental analyzer attached to a Finnigan MAT 253 isotope ratio mass spectrometer. All δD data were normalized to VSMOW (Vienna-Standard Mean Ocean Water) using certified reference standards "USGS57 biotite" (−90.996‰) and "USGS58 muscovite" (−27.999‰, Qi et al., 2017). Repeated δD measurements of standards yielded an analytical precision of ±1.8‰ for Tephras 1, 2, and 3 and ±2.4‰ for Tephras 5, 6, 7, 8.1, 8.2, 8.3, 9, 10.1, 10.2, 10.3, and 11; all samples were run in duplicate. Water content was measured from the Finnigan MAT 253 mass spectrometer via peak integration with reference standards "NBS30" ($H_2O = 3.5$ wt%) or "USGS58 muscovite" ($H_2O = 3.5$ wt%), following procedures from Martin et al. (2017).

2.4. δD_{precip} Estimates

δD_{glass} is offset from the δD of secondary hydration waters ($\delta D_{environmental\ water}$) due to isotopic fractionation that occurs during diffusion. As defined by Friedman, Gleason, Sheppard, and Gude (1993), Equation 1 provides a reasonable approximation of net fractionation between rhyolitic glasses and secondary waters and has been applied by previous studies (e.g., Cassel & Breecker, 2017; Colwyn et al., 2019; Dettinger & Quade, 2015; Friedman, Gleason, & Warden, 1993; Mulch et al., 2008).

$$\delta D_{environmental\ water\ (or\ precip)} = 1.0343 \times \left(1000 + \delta D_{glass}\right) - 1,000. \quad (1)$$

We make the assumption that $\delta D_{environmental\ water}$ is representative of the mean isotopic composition of precipitation-fed environmental waters that interact with shallowly buried tephras in the Alaska and Yukon region. However, we recognize that $\delta D_{environmental\ water}$ values are influenced by topographic and site-specific factors that include slope, aspect, ground thermal regime, microtopography, and vegetation, which further influence the hydrological regime and residence times of meteoric water from different seasons in the shallow groundwater zone. Additionally, the isotopic value archived in volcanic glass integrates a multi-thousand-year average signal that therefore incorporates variations in the δD value of the original rainfall, which owes to changes in the water source, air temperature, and elevation.

2.5. δD_{precip} Corrections and Uncertainty

Over glacial–interglacial and Cenozoic timescales, precipitation isotope ratios are influenced by the isotopic composition of seawater (δ_{SW}), which varies due to changes in water storage between the global ocean and land ice. To isolate δD_{precip} signals recorded in the tephra record that are potentially related to regional

climate change, it is necessary to correct paleo-δD_{precip} estimates for long-term changes in δD_{SW}. Seawater-corrected δD_{precip} estimates are calculated as outlined in Equation 2 (modified from Stenni et al., 2011) as follows:

$$\delta D_{precip-corrected} = \delta D_{precip} - \delta D_{SW} \times \left(1 + \delta D_{precip}/1,000\right)/\left(1 + \delta D_{SW}/1,000\right). \quad (2)$$

Long-term changes in δD_{SW} are assumed based on reconstructed $\delta^{18}O_{SW}$ changes over the last 5.3 Ma (Rohling et al., 2014) and assuming that changes in δD_{SW} are eight times larger than changes in $\delta^{18}O_{SW}$ (i.e., consistent with the global meteoric water line; Craig, 1961). The latter assumption is supported by direct measurements of δD_{SW} and $\delta^{18}O_{SW}$ from pore waters dating to the last glacial maximum (Schrag et al., 2002) and is commonly assumed in ice core (Stenni et al., 2011) and relict permafrost (Porter et al., 2019) studies. For δD_{precip} estimates prior to 5.3 Ma—which applies to the Gunn Creek and Grubstake tephras (6.7–5.8 Ma)—we assume a constant $\delta^{18}O_{SW}$ of −1.28‰ (the reconstructed value for 5.3 Ma BP; (Rohling et al., 2014) and 8:1 relationship between δD_{SW} and $\delta^{18}O_{SW}$. The assumption of a static seawater isotopic composition between ~6.7 and ~5.3 Ma is thought to be reasonable as there are no major shifts in reconstructed sea level or benthic foraminifera $\delta^{18}O$ (Zachos et al., 2001) through this interval of time.

For each δD_{precip} estimate, we report the compound or total uncertainty, calculated as outlined in Equation 3 as follows:

$$\sigma_T = \left(\sigma_A{}^2 + \sigma_{SV}{}^2 + \sigma_{SW}{}^2\right)^{1/2}, \quad (3)$$

where σ_T is the total uncertainty, σ_A is the analytical uncertainty, σ_{SV} is intra-site variability (i.e., the standard deviation where multiple replicates of the same tephra were analyzed), and σ_{SW} is uncertainty in δD_{SW} (as determined by the dating uncertainty of the tephra).

Finally, because the tephras included in this study are from multiple sites across the study region, some of the variability in reconstructed δD_{precip} will be expected from spatial variability in the precipitation isoscape. These site-specific differences were normalized by expressing the seawater-corrected δD_{precip} values as anomalies ($\Delta\delta D_{precip}$) relative to the modern mean annual δD_{precip} for each site, estimated using the Online Isotopes in Precipitation Calculator (Bowen & Revenaugh, 2003; IAEA/WMO, 2018).

2.6. Extraction and LCMS/MS Analysis of GDGTs

Sediment samples (mudstone, lignite, and sandstone) were collected within 1 to 4 m above and below each ash bed for a total of four to nine samples from Sites 5, 6, 8, and 10. The number of viable samples for biomarker analysis varied depending on lithology. Sufficient brGDGT yields were associated with fine-grained sediments—mudstones and lignite samples (Table 1)—whereas coarse-grained sediments had insufficient yields for brGDGT analysis. The samples were kept at ambient temperatures in the field and, once shipped to the University of Toronto, immediately frozen in order to reduce potential bacterial overprinting.

The sediment samples were freeze dried (Labconco Freezone 2.5 unit) and homogenized using a mortar and pestle prior to solvent-lipid extraction. A total lipid extract (TLE) was recovered from approximately 7 g of each sample by microwave assisted (Ethos Up Microwave) solvent extraction using 25 mL of 9:1 (v:v) Dichloromethane (DCM): Methanol (MeOH). The TLE was then separated into the polar and GDGT-containing apolar fraction by column chromatography using an aminopropylsilyl-gel column. The GDGT fraction was eluted with a 2:1 (v:v) DCM:isopropanol mobile phase and then condensed under a gentle stream of high-purity, dry nitrogen gas. This was followed by re-dissolving the GDGT fraction in hexane:propanol 99:1 and then filtering the solution through 0.45 mm PTFE membrane filters into autosampler vials.

Chromatographic separation of GDGTs was achieved on an Agilent Technologies 1290 Series II ultra-pressure liquid chromatograph coupled to an AB Sciex 4500 QTrap triple quadrupole mass spectrometer, using a method based on Hopmans et al. (2016). We utilized two 150 mm × 2.1 mm BEH HILIC (1.7 μm) columns (Waters Corporation) linked in series and fitted with a 2.1 mm × 5 mm precolumn of the same sorbent. Based on Tierney (2012), selected ion monitoring for specific branched chain, and isoprenoidal GDGTs was configured to detect quasimolecular $(M + H)^+$ ions at m/z 1018 (brGDGT-Ic), 1020

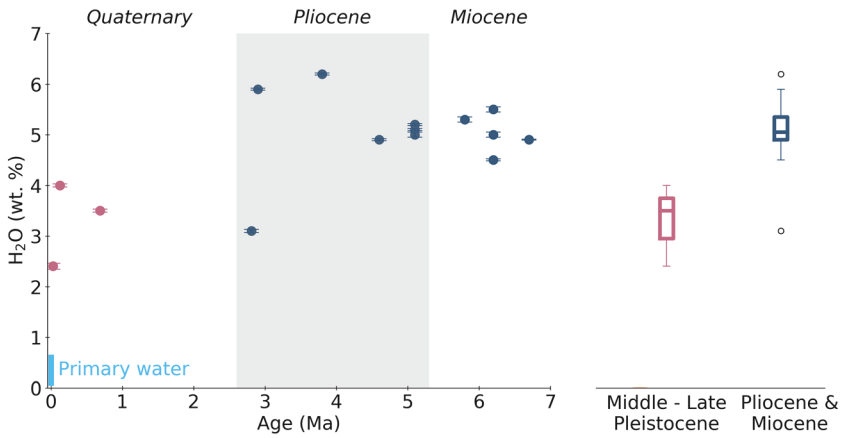

Figure 2. Age and hydration (wt% H_2O) of the sampled tephras included in this study. Pleistocene datapoints are colored red and Miocene–Pliocene datapoints are colored blue. The boxplots summarize the Pleistocene and Miocene–Pliocene tephra hydration values. The range of initial hydration values for a tephra at the time of eruption (i.e., 0 Ma) is indicated with a blue line (Seligman et al., 2016).

(brGDGT-Ib), 1022 (brGDGT-I), 1032 (brGDGT-IIc), 1034 (brGDGT-IIb), 1036 (brGDGT-II), 1046 (brGDGT-IIIc), 1048 (brGDGT-IIIb), 1050 (brGDGT-III), 1292.2 (crenarcheol), 1296.2 (GDGT-3), 1298.3 (GDGT-2), 1300.3 (GDGT-1), and 1302.3 (GDGT-0). All samples were normalized to sample mass.

The brGDGTs data were used to calculate the temperature-sensitive MBT'_{5me} index using Equation 4, as defined by De Jonge et al. (2014). The MBT'_{5me} index measures the relative abundance of tetramethylated (Ia-Ic), pentamethylated (IIa-IIc), and hexamethylated (IIIa-IIIc) brGDGTs from the 5-methyl isomers as follows:

$$MBT'_{5Me} = (Ia + Ib + 1c)/(Ia + Ib + Ic + IIa + IIb + IIc + IIIa + IIIb + IIIc. \quad (4)$$

Reported uncertainties associated with the MBT'_{5me} index values were calculated according to Equation 5 as follows:

$$\sigma_T = \left(\sigma_A{}^2 + \sigma_{SV}{}^2\right)^{1/2}, \quad (5)$$

where σ_T is the total uncertainty, σ_A is the analytical uncertainty, and σ_{SV} is one standard deviation of intra-site variability associated with the independent MBT'_{5me} measurements at a given site. Unlike the $\Delta\delta D_{precip}$ estimates, no attempt was made to correct for potential spatial differences in MBT'_{5me} values due to a lack of modern MBT'_{5me} data from the study region. Differences between sites might be expected if there were spatial differences in mean climate. However, all of the sites with MBT'_{5me} data have roughly the same mean temperature, and so temporal differences in the MBT'_{5me} index are interpreted as a change in mean temperature from a common baseline.

3. Results

The glass shards of the sampled tephras showed a range of water content from 2.3 to 6.2 H_2O wt% (Table 1; Figure 2). The Pliocene and Miocene volcanic glasses have a mean hydration value of 5.0 ± 0.8 wt% ($n = 12$). Only one of the Pliocene samples—Quartz Creek tephra (Tephra 4)—which is hydrated to 3.1 wt% diverges significantly from the average of 5.0 ± 0.8 wt%. The late Pleistocene glasses (mean wt% $= 3.3 \pm 0.7$, $n = 3$) are significantly less hydrated than the Miocene and Pliocene mean hydration value (t-Stat $= -3.16$, $p = 0.03$). The Dawson tephra, especially, which is the youngest tephra (29.4 cal ka BP), has the lowest hydration value of 2.3 wt%.

The seawater corrected $\Delta\delta D_{precip}$ values range from −27‰ to +30‰ (Table 1; Figure 3a). Late Miocene $\Delta\delta D_{precip}$ values decrease from +20‰ at 6.7 Ma (Tephra 11) to −14‰ at 6.17 Ma (average of Tephra 10), then to −24‰ at 5.86 Ma (Tephra 9). The reconstruction then indicates an increase during the transition to the

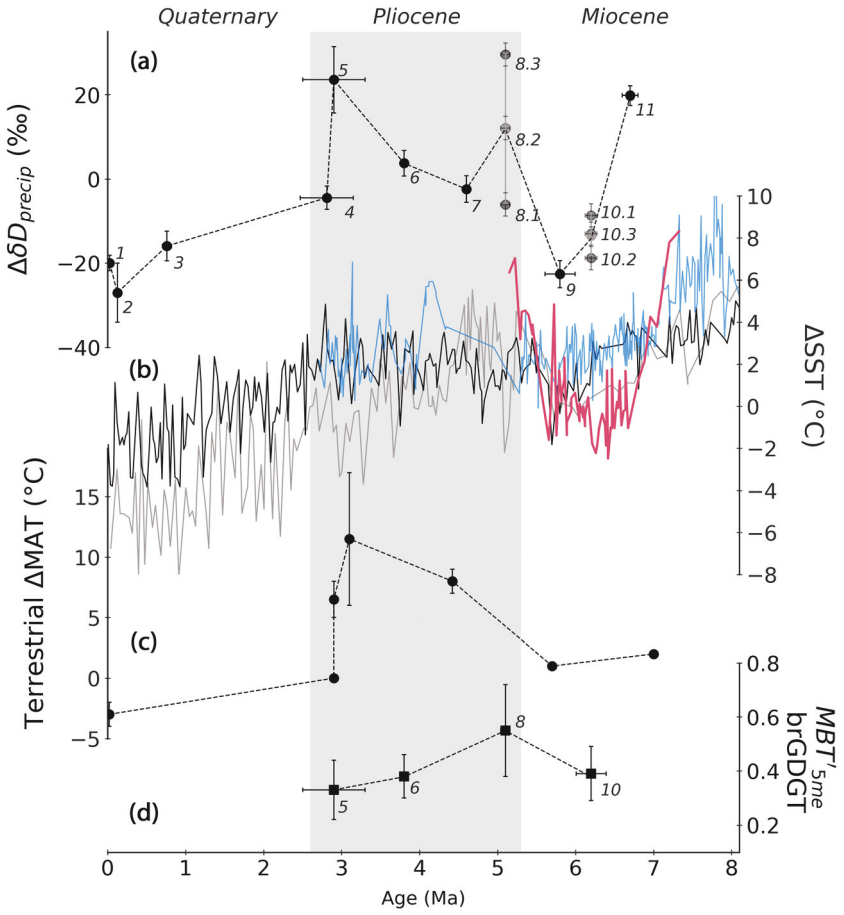

Figure 3. (a) Volcanic glass-based $\Delta\delta D_{precip}$ estimates (this study; site/tephra numbers correspond to Table 1). (b) North Pacific Sea Surface Temperature (SST) reconstructions expressed relative to modern from Ocean Drilling Program sites 883/884 (blue), 887 (red), 1021 (gray), and 1208 (black; Herbert et al., 2016). (c) Previous temperature estimates in central Alaska and Yukon (Table 3). (d) MBT'_{5me} indices for Sites 5, 6, 8, and 10 (this study; Table 2).

early Pliocene with $\Delta\delta D_{precip}$ values increasing in stratigraphic sequence (oldest to youngest) from −6 to +30‰ at approximately 5.08 Ma (Tephra 8). Middle Pliocene $\Delta\delta D_{precip}$ estimates are similar to modern and range from −2‰ (4.63 Ma, Tephra 7) to +4‰ (3.81 Ma, Tephra 6). High variability in $\Delta\delta D_{precip}$ is observed in the late Pliocene with mean values ranging from +24‰ (2.91 Ma, Tephra 5) to −4‰ (2.81 Ma, Tephra 4). Finally, the late Pleistocene tephras (0.74 to 0.03 Ma) indicate lower $\Delta\delta D_{precip}$ values ranging between −27 and −16‰ (Tephras 1, 2, and 3).

brGDGTs were detected in sediment samples from Lost Chicken and three of the EAR localities—Phelan Creek, Proposal Creek, and "Upper" Gunn Creek. Sediments from McCallum Creek were highly oxidized and did not yield detectable brGDGTs. The mean MBT'_{5me} index values (Table 2) range from 0.29 ± 0.1 to 0.55 ± 0.17.

Table 2
Average MBT'_{5me} Index Values for Tephras/Sites 5, 6, 8, and 10

Location	Site/tephra	MBT'_{5me}	Associated tephra age (ma)
Lost Chicken	5	0.33 ± 0.11 (n = 9)	2.91 ± 0.44
Phelan Creek	6	0.37 ± 0.08 (n = 5)	3.81 ± 0.05
Proposal Creek	8	0.52 ± 0.17 (n = 4)	5.08 ± 0.06
Gunn Creek	10	0.39 ± 0.10 (n = 4)	6.17 ± 0.08

4. Discussion

4.1. Tephra Hydration

Our dataset shows a statistically significant difference in hydration percentage between the Miocene–Pliocene tephras and the late Pleistocene tephras (Figure 2). This could be interpreted to mean that these volcanic glasses continued to take on water throughout their burial history, thereby continuously diluting environmental water δD signals from the time of deposition, which are typically of interest in tephra-based

δD_{precip} reconstruction studies. If true, this result would contradict previous research that has demonstrated no significant association between age and H_2O wt% after ~2,000 years (Seligman et al., 2016). However, we argue that the relatively low H_2O wt% values of the late Pleistocene tephras are more likely explained by special depositional circumstances in syngenetic (aggrading) permafrost. The Dawson tephra at Goldbottom Creek, which is up to 80 cm thick (Froese et al., 2006), may have been fully entombed in syngenetic permafrost within 400 years of deposition (Porter et al., 2016). It is also possible that the low temperatures associated with these depositional sites reduced the diffusion rate of water into the late Pleistocene glasses. This depositional circumstance, with subfreezing temperatures and lower availability of liquid water in comparison to the unfrozen active layer, is likely important to explaining the low hydration value of glass shards in this tephra. The other Pleistocene tephras—Old Crow tephra at ThC (Reyes et al., 2010) and Gold Run tephra at Dominion Creek (Westgate et al., 2009)—were likewise recovered from syngenetic permafrost sections driven by loess accumulation and may have shared a similarly rapid burial history.

The saturation or hydration limit of glass shards is debated in the literature and can be highly variable, with reported values ranging from 3–6 wt% H_2O (Cassel & Breecker, 2017; Dettinger & Quade, 2015; Friedman et al., 1992; Leschik et al., 2004; Martin et al., 2017; Mulch et al., 2008), a range that encapsulates most of our glass shard samples. However, clearly the late Pleistocene samples have undergone less hydration compared with the Miocene–Pliocene samples (~5–6 wt.%). It is unlikely that this difference in water content owes to glass morphology as no major differences were observed optically. Similarly, this difference is not due variations in glass geochemistry as all volcanic glass samples are rhyolitic, with the exception of Tephra 10.1 which has a slightly dacitic geochemistry. It is most probable that the entombment of the Pleistocene tephras in permafrost shortly after deposition is responsible for their lower hydration values.

4.2. Reconstructed $\Delta\delta D_{precip}$ and Inferred Climate

The reconstructed trends in $\Delta\delta D_{precip}$ can be largely explained by changes in North Pacific regional temperatures over the past ~7 Myr, and changes in the topography of southern Alaska may also be playing a partial role. Other factors independent of elevation and climate are also known to influence glass-based $\Delta\delta D_{precip}$ estimates. For example, the isotopic composition of volcanic glass may be altered by exposure to high burial temperatures at depths greater than 2 km (Dettinger & Quade, 2015). Opportunely, the Miocene and Pliocene tephra beds utilized in this study have undergone comparatively shallow burial of <2 km (Allen, 2016; Triplehorn, 1976; Wahrhaftig et al., 1969) and therefore $\Delta\delta D_{precip}$ variability in our samples is likely unaffected by burial. Within this framework, the following discussion outlines the most probable influence that elevation has had on precipitation isotopes over the study interval. We then discuss the possible climatic origins of reconstructed $\Delta\delta D_{precip}$ variability and coherency between regional temperature records and our $\Delta\delta D_{precip}$ reconstruction, which is also supplemented by additional factors that may have influenced precipitation isotopes since the late Miocene.

Elevation influences ambient temperatures and distillation of precipitation isotopes (Dansgaard, 1964). As an airmass traverses a mountain range, the moist air will undergo enhanced rainout of heavy isotopologues as it ascends due to adiabatic cooling, with an approximate decrease in δD_{precip} of $-21‰ \cdot km^{-1}$ (Poage & Chamberlain, 2001). This relationship has been exploited to reconstruct paleo-elevation in other mountains around the world over longer timescales throughout the Cenozoic (Canavan et al., 2014; Cassel et al., 2014; Colwyn et al., 2019; Fan et al., 2014; Mulch et al., 2008). Such studies infer changes in mean elevation based on the difference between modern- and paleo-topographic profiles of δD_{precip}. However, the tenability of this approach in the Alaskan Range has not been assessed. That said, thermochronology studies indicate a change in the mean exhumation rate of the Alaskan, Chugach, and St. Elias ranges since ~30 Ma (Benowitz et al., 2011, 2014; Enkelmann et al., 2008, 2010; Lease et al., 2016; Trop et al., 2019). Similarly, initiation of Wrangel Arc volcanism began at ~30 Ma, which marks the initial development of the Wrangel's high volcanic peaks (Berkelhammer et al., 2019; Brueseke et al., 2019). By 18 Ma, continued uplift of the Central Alaska range was sufficient enough to trigger the reorganization of the formerly south-flowing Nenana drainage system (Benowitz et al., 2019). At ~10 Ma, rapid exhumation of the St. Elias Mountains commenced, which is interpreted as uplift responsible for the onset of alpine glaciation by 6–5 Ma (Enkelmann et al., 2017). Although the magnitude of topographic change in southern Alaska by 7 Ma is currently unknown, evidence suggests that the mountain ranges in southern Alaska had developed as significant orographic barriers by the beginning of our record. As a driver of precipitation isotope change, the

Table 3
Quantitative Reconstructions Of Mean Annual Temperature Anomalies From Yukon and Alaska

Age (Ma)	Site	Proxy	ΔMAT (°C)	Citation
0.02	E. Beringia region	Pollen	−2 to −4	Viau et al. (2008)
2.9	Lost Chicken, Alaska	Insects*	0	Elias and Matthews (2002)
2.9	Lost Chicken, Alaska	Pollen*	+5 to +8	Matthews et al. (2003)
3.6 to 2.6	Klondike, Yukon	Pollen	+6 to +17	Pound et al. (2015)
4.42[a]	Terrace gravels, Circle, Alaska	Pollen	+7 to +9	Ager et al. (1994)
4.42[a]	Nenana gravels, Alaska	Pollen	+7 to +9	Ager et al. (1994)
5.7	Lava Camp, Alaska	Insects*	+1	Elias and Matthews (2002)
7	Kenai, Alaska	CLAMP[b]	+2	Wolfe (1994)
8.5	Kenai, Alaska	CLAMP[b]	+2	Wolfe (1994)

*Average of reconstructed warmest-month and coldest-month temperature anomalies (rel. to present). [a]Cosmogenic burial age of 4.42 + 0.67/−0.13 Ma for the Lower Nenana gravels (Sortor et al., 2017). [b]ΔMAT was calculated from absolute MAT estimates assuming a modern MAT of 3.7°C at Homer, Alaska (applies to the Seldovian and Homerian CLAMP estimates), and a modern MAT of 1.2°C for Clamgulch, Alaska (applies to the Clamgulchian CLAMP estimates).

continuous uplift of the mountain ranges in southern Alaska since ~30 Ma has likely caused a continual depletion of mean δD_{precip} at sites in the rainshadow of the coastal range. Although the magnitude of elevation gains is unknown, we assume some decrease in our $\Delta\delta D_{precip}$ record since 6.7 Ma is due to gradual uplift. However, increases in reconstructed $\Delta\delta D_{precip}$, as observed during the Miocene–Pliocene transition and the transition from Late Pleistocene and the 0‰ baseline, are unlikely related to changes in mean elevation because that would require significant reduction in the orographic barrier, which is unlikely to occur in the Alaska Range—a documented compressional, actively uplifting mountain range (Waldien et al., 2018). As such, climatic factors are inferred to play the major role in driving variability in this isotopic record.

The late Miocene decrease of $\Delta\delta D_{precip}$ to values that are negative with respect to modern (Table 1; Figure 3a) implies a possible cooling trend to a mean climate that was colder than modern. Cooling trends through this interval are observed in both qualitative growing-season temperature estimates based on pollen from Alaskan sites (White et al., 1997) as well as extratropical ΔSST reconstructions from the North Pacific based on the alkenone-unsaturation index (Figure 3b; Herbert et al., 2016). However, a late Miocene climate that was cooler than modern is refuted by most ΔSST reconstructions (Figure 3b), which suggest warmer-than-modern ΔSST throughout the late Miocene, with the exception of some locations that record brief excursions to values as low as ~2°C colder than modern ΔSST (e.g., ODP887; Figure 3b). Moreover, fossil insect assemblages indicate a MAT anomaly estimate of approximately +1°C, dating to 5.7 Ma from Lava Camp Mine, N.W. Alaska. (Table 3; Elias & Matthews, 2002). Given the balance of independent temperature proxy data, the trend towards cooler temperatures in the late Miocene is supported by other independent climate proxy evidence, but the reconstructive negative mean $\Delta\delta D_{precip}$ values suggest other factors unrelated to changes in mean temperature were also involved.

To some extent, the decrease in $\Delta\delta D_{precip}$ values between 6.7 and 5.86 Ma is consistent with an uplift scenario, which is supported by increased exhumation rates in the central Alaska Range at ~7–6 Ma (Fitzgerald et al., 1993) and in the St. Elias Range since ~10 Ma (Enkelmann et al., 2017). However, if $\Delta\delta D_{precip}$ was driven only by elevation, negative mean $\Delta\delta D_{precip}$ values would imply that elevations during the late Miocene were higher than they are today, which is not supported by other studies (Benowitz et al., 2011; Waldien et al., 2018). Alternatively, negative $\Delta\delta D_{precip}$ could represent a mean climate at this time that was significantly colder than modern. However, this scenario is also not supported by other studies (e.g., Herbert et al., 2016; Wolfe, 1994). Instead, the negative $\Delta\delta D_{precip}$ estimates may owe to differences in precipitation isotope-influencing ocean and atmospheric circulation patterns.

North Pacific atmospheric circulation patterns exert a strong influence on precipitation seasonality (Mock et al., 1998) and mean precipitation isotope composition (Field et al., 2010) in the areas of Yukon and Alaska. Accordingly, the alteration of atmospheric circulation patterns through time is an important influence on the isotopic composition of precipitation, as is discussed in detail in the ice core literature (e.g., Field et al., 2010). Consequently, precipitation isotope records must be interpreted within the context of dynamic

boundary conditions such as land–ocean configurations, which influence moisture source and precipitation seasonality in Alaska and Yukon. This is because changes to land–ocean configurations can modify the continentality of the Western Arctic region, which alters pressure field and moisture trajectories that lead into Alaska and Yukon and ultimately affects moisture source and precipitation seasonality.

Over the last 7 Myr, significant changes to land–ocean configurations include the first flooding of the Bering Strait at 5.5–5.4 Ma (Gladenkov et al., 2002), the collapse of the contiguous continental Arctic Archipelago in the Pleistocene (England, 1987), and variability in eustatic sea levels (Rohling et al., 2014). In addition, it is likely that δD_{precip} was influenced by local-scale changes such as the development of alpine glaciers in the St. Elias range by 6–5 Ma (Zellers, 1995). For example, the growth of alpine glaciers could have a strong effect on the local surface energy balance, which would lead to cooling and therefore enhanced rainout of heavy isotopologues. The combination of local and regional boundary conditions changes, with possible influences on atmospheric circulation, are currently poorly constrained but could be explored further by future analysis of isotope-enabled global circulation models equipped with latest Miocene boundary conditions.

The increase of $\Delta\delta D_{precip}$ estimates into the Pliocene can be partially explained by a simultaneous warming trend indicated by other proxies. All three ΔSST reconstructions with full Pliocene coverage (ODP 883/884, 1021 and 1208; Figure 3b; Herbert et al., 2016) show strong warming trends starting around 5.7 Ma. Moreover, early Pliocene ΔSST were generally warmer than latest Miocene (prewarming) ΔSST (Herbert et al., 2016). Similarly, insect and pollen assemblages from northeastern Alaska indicate increased MATs in Alaska from 5.7 to 4.42 Ma (Table 3, Figure 3c; Ager, 1994; Elias & Matthews, 2002). Warming over the Mio-Pliocene transition is also indicated from our brGDGT data (Table 2), which indicate a significant increase of MBT'_{5me} values ($t = -1.76$, $df = 6$, $p = 0.06$) from Gunn Creek (6.17 Ma, Site 10) to Proposal Creek (5.06 Ma, Site 8) of 0.13. As a general rule, more positive MBT'_{5Me} indices can be interpreted to mean warmer conditions. However, absolute temperature estimates based on MBT'_{5Me} are sensitive to the MBT'_{5Me}-temperature transfer function that is used (e.g., Dang et al., 2018; Naafs et al., 2017; Russell et al., 2018), which can depend on depositional setting and region, as well as the source of brGDGTs (De Jonge et al., 2014; Russell et al., 2018). As of yet, there are no calibrations for this specific study region or depositional setting and, therefore, we refrain from quantitative temperature estimates and instead use the MBT'_{5Me} index mainly for qualitative temperature inferences.

Although climate warming is likely a key factor driving the Mio-Pliocene increase in reconstructed $\Delta\delta D_{precip}$ values, other nonclimatic factors such as isotope effects from the opening of the Bering Strait at ~5.5–5.4 Ma may be involved (Gladenkov et al., 2002). Additionally, the depositional setting of the tephras can also be important. For example, closed-basin lakes are susceptible to evaporation which preferentially removes light isotopologues, thereby enriching the isotopic composition of lake waters (Cassel & Breecker, 2017; Dettinger & Quade, 2015; Quade et al., 2007). Analysis of modern closed-basin lakes in this region indicates up to ~40–50‰ enrichment of lake water δD relative to unenriched source waters (Anderson et al., 2016). As such, multiple tephras deposited in close succession of one another within a developing closed-basin lake would inherit a successively more enriched isotopic composition. This isotopic enrichment scenario may explain the up-section increase of $\Delta\delta D_{precip}$ estimates from Tephras 8.1, 8.2, and 8.3 (Figure 3a), which were deposited in close-stratigraphic succession and similar lacustrine sediments (Table 1; Allen, 2016), although the hydrologic connectivity of this depositional environment remains unknown. All evidence considered, increasing $\Delta\delta D_{precip}$ estimates during the Mio-Pliocene transition appear to reflect regional warming, which is coincident with relatively high global pCO_2 concentrations (Beerling & Royer, 2011). This coherence may further support the importance of greenhouse gas forcing in developing warm climate throughout the Cenozoic, which was suggested by Anagnostou et al. (2016).

The coarse resolution of the $\Delta\delta D_{precip}$ record from this study precludes interpretations of high-frequency climate oscillations because of the relatively long hydration interval and uncertainty associated with radiometric dating. However, our $\Delta\delta D_{precip}$ reconstruction does indicate high variability throughout the Pliocene epoch, which may indicate variable climatic conditions. Higher than modern $\Delta\delta D_{precip}$ estimates from Lost Chicken (Tephra 5) indicate very warm temperatures at 2.91 Ma, and high temperatures are also observed in MAT reconstructions derived from pollen records in central Alaska (Matthews et al., 2003). Pollen-based temperature estimates from this region are ubiquitously warm during the middle to late Pliocene (4.42 to 2.6 Ma) ranging from 5 to 17°C warmer than present (Table 3, Figure 3(c); Ager

et al., 1994; Ager, 1994; Matthews et al., 2003; Pound et al., 2015). Even warmer Pliocene conditions have been reconstructed in parts of the Canadian High Arctic based on a range of biological and geochemical proxies (Ballantyne et al., 2010; Csank, Patterson et al., 2011; Csank, Tripati et al., 2011; Elias & Matthews, 2002). Conversely, climatic conditions that were similar to present during the Pliocene are indicated by volcanic glass derived from McCallum Creek (Tephra 7) and Phelan Creek (Tephra 6). Moreover, slightly colder conditions are indicated by glass from the Quartz Creek ash bed (Tephra 4). However, independent proxy evidence also supports cooler intervals during the Pliocene in central Yukon based on the presence of ice-wedge casts found in the Upper White Channel gravels of the KD, the same sedimentary unit containing the Quartz Creek tephra (Froese et al., 2000; Westgate et al., 2002). The Quartz Creek tephra was cobedded in the sediment infill of an ice-wedge cast, indicating that this tephra was deposited at a time when permafrost was present, which precludes a climate that was much warmer than today. This is because both ground-ice features are common to regions where MATs are only as warm as −4°C (Burn, 1990), which is similar to the modern MAT (1981–2010) of Dawson City, the closest climate station to the Quartz Creek tephra (−4.1°C).

In general, the trends in our volcanic glass-derived $\Delta\delta D_{precip}$ record from Pliocene ash beds are similar to trends observed in independent temperature proxy records from Alaska and Yukon. Moreover, average Pliocene $\Delta\delta D_{precip}$ estimates (Tephras 4–8) are higher than those during the latest Miocene (Tephras 9–10) as well as modern values. Although $\Delta\delta D_{precip}$ estimates are subject to uncertainty related to local and regional scale isotopic influences, the average Pliocene $\Delta\delta D_{precip}$ value is 7‰ higher than modern. This anomaly translates to an average Pliocene climate that was 3.9 ± 1.3°C warmer than modern, assuming a 1.8 ± 0.19‰ $°C^{-1}$ transfer function (Supporting Information). There are some ambiguities that persist between the terrestrial proxies from this region, as is the case for Lost Chicken (Tephra 5). The tephra-based $\Delta\delta D_{precip}$ record (Figure 3a) and pollen-based estimates (Table 3) imply a MAT that was much warmer than today, whereas fossil beetle estimates suggest a MAT that was approximately equivalent to today (Table 3). Moreover, brGDGTs imply a cooler climate associated with Lost Chicken in comparison with earlier Pliocene sites at 3.81 Ma (Site 6) and at 5.08 Ma (Site 8). The mean MBT'_{5Me} index value observed for Lost Chicken (0.33 ± 0.11; Site 5) is significantly lower (t-Stat = −3.25, $df = 6$, $p \leq 0.01$) than the early Pliocene MBT'_{5Me} value constrained by Proposal Creek (0.52 ± 0.17; Site 8; Table 2; Figure 3d). Overall, these proxies do not provide a clear record of climatic conditions in continental Alaska and Yukon during the late Pliocene. Thus, we conclude that the late Pliocene climate of this region is a topic that deserves further research to better understand, which may be resolved based on additional replication from other tephras and other independent multiproxy approaches.

The $\Delta\delta D_{precip}$ estimates from late Pleistocene tephras are defined by an average −21‰ relative to modern, some of the most negative values in our composite record and which suggests a cooler-than-modern climate at the time of deposition. This is a reasonable interpretation given that sedimentary data suggest the Dawson tephra (Froese et al., 2006), Old Crow tephra (Reyes et al., 2010), and Gold Run tephra (Westgate et al., 2009) were deposited during cool climatic intervals, but not necessarily full-glacial stages (Froese et al., 2009). Compared with modern, periods of colder and drier conditions in Eastern Beringia during the late Pleistocene are indicated by a range of paleoecological and sedimentological indicators (Elias, 2001; Jensen et al., 2016; Muhs et al., 2018; Viau et al., 2008; Zazula et al., 2003). However, the average $\Delta\delta D_{precip}$ estimate from the late Pleistocene tephras indicates a climate that was ~12 ± 3.2°C cooler than modern while other temperature records show slightly warmer conditions. For example, pollen-based estimates for the late last glacial (~25–16 ka BP) indicate that January and July mean temperatures were up to 4°C and 2°C colder than modern, respectively (Viau et al., 2008). Similarly, fossil beetle assemblages indicate that warm-season temperatures during Marine Isotope Stages 4 to 2 were approximately 2°C to 6°C colder than today in interior Alaska and Yukon (Elias, 2001). A cooler-than-modern late Pleistocene is also well supported by the North Pacific ΔSST reconstructions from ODP sites 1021 and 1208 (Herbert et al., 2016). Both of these records show prominent cooling trends since the Pliocene-Pleistocene transition and negative ΔSST values through most of the last ~1 Ma. However, the magnitude of cooling in the North Pacific may have been spatially variable; for example, over the last 1 Ma, the mean ΔSST reconstructed was −5.2 ± 1.8°C for ODP site 1021 (E. North Pacific) and −1.9 ± 1.4°C for ODP site 1208 (W. North Pacific; Figure 3b). These depressions are consistent with the range of temperature depressions indicated by fossil pollen and insects and therefore substantiate cooler-than-modern conditions during the latest Pleistocene,

but climate alone cannot account for the magnitude of $\Delta\delta D_{precip}$ depletion at this time. As such, the negative $\Delta\delta D_{precip}$ estimates during the late Pleistocene most probably owe to factors other than climate.

Past research indicates that seasonal precipitation amounts during the Pleistocene were different in comparison with modern regimes, in Alaska and Yukon. For example, past reconstruction of central Yukon precipitation $\Delta\delta D_{precip}$ values associated with the Dawson tephra (Tephra 1) at 0.029 Ma indicate that the presence of the Greenland and Laurentide Ice Sheet during the Last Glacial Maximum resulted in a net reduction in both cold- and warm-season precipitation totals but a stronger decrease in summer than in winter resulting in a more negative annual precipitation isotope composition (Porter et al., 2016). The opposite precipitation seasonality change is thought to have occurred over Greenland, with summer precipitation accounting for a greater fraction of the annual precipitation budget during the full glacial (Johnsen et al., 2001). In our study region, the implication of a more winter-biased precipitation seasonality is that the Pleistocene tephras may reflect a more negative isotopic composition, as observed in our record. Overall, the Pleistocene tephra values are consistent with a climate that was significantly colder than modern, as reflected in a range of multiproxy evidence, but the magnitude of this depletion is perhaps greater than expected, which may relate to changes in precipitation seasonality driven by changes in glacial and stadial boundary conditions.

5. Conclusion

This study produced the first reconstruction of $\Delta\delta D_{precip}$ (difference relative to modern δD_{precip}) spanning the last ~7 Myr based on the δD of hydrated volcanic glass shards from tephras in the Alaska Range and continental Alaska-Yukon. A general pattern emerges from this record showing a decreasing trend in $\Delta\delta D_{precip}$ values during the latest Miocene, culminating in mean values that are negative compared with the modern baseline, followed by an increase to higher-than-modern average $\Delta\delta D_{precip}$ values during the Pliocene, and then a decrease to lower-than-modern average values in the Middle and Late Pleistocene. We interpret this pattern to reflect a generally warmer-than-modern climate in the Pliocene followed by a cooler climate in the Pleistocene, as supported by most other biological proxies in this region. Qualitative temperature estimates based on the brGDGT-derived MBT'_{5ME} index also indicate a significantly warmer climate during the early Pliocene compared with the middle to late Pliocene. However, the magnitude of reconstructed $\Delta\delta D_{precip}$ changes is also likely influenced in part by factors that are unrelated to mean climatic temperatures, which vary at both local scales (e.g., depositional environment, burial history, and paleo-elevation) and regional scales (e.g., ocean–atmosphere boundary conditions). To better control for these uncertainties, future studies are needed to enhance the replication of this record through the discovery and analysis of new tephras and application of paleoaltimetry and numerical modeling techniques. More quantitative applications of the MBT'_{5me} brGDGT index to the late Cenozoic sedimentary record of Yukon-Alaska may also be possible in future studies but should be based on a local temperature-MBT'_{5me} calibration that is representative of the fluvial and lacustrine depositional settings in Yukon and Alaska today. Nevertheless, this study demonstrates the viability of developing fossil biomarker and volcanic glass-derived $\Delta\delta D_{precip}$ reconstructions in this region and diversifying the proxies available for paleoclimate research in Alaska-Yukon, which to date has primarily been limited to biological proxies (e.g., fossil pollen and insects).

Data Availability Statement

All tephra δD_{glass}, MBT'_{5Me}, and supplemental tephra geochemistry data generated in this study can be accessed from the Polar Data Catalogue (https://polardata.ca), CCIN reference number 13114.

Acknowledgments

The authors thank Editor Ellen Thomas, Gabriel Bowen, Elizabeth Cassel, and one anonymous reviewer for feedback that improved the paper. We acknowledge Sydney Clackett, Aleesha Bakkelund, Paul Fitzgerald, Ken Ridgway, Kailyn Davis, and Wai Allen for fieldwork assistance and Kira Holland for comments on earlier drafts of the manuscript. The authors acknowledge the support of funding agencies: Northern Science and Training Program grant to G. Otiniano, NSERC Discovery Grant and University of Toronto Connaught New Researcher Award to T. Porter, NSF award to J. Benowitz (1434656 and 1550123) to Bindeman (EAR1822977), and Discovery Grant to Canada Research Chair D. Froese.

References

Ager, T. A. (1994). Terrestrial Palynological and Paleobotanical Records Of Pliocene Age From Alaska and Yukon Territory (Open-File Report No. 94–023). U.S. Geological Survey. Retrieved from https://pubs.usgs.gov/of//1994/of94-023/02_Ager.html

Ager, T. A., Matthews, J. V., & Yeend, W. (1994). Pliocene terrace gravels of the ancestral Yukon River near Circle, Alaska: Palynology, paleobotany, paleoenvironmental reconstruction and regional correlation. *Quaternary International*, *22*, 185–206.

Allen, W. (2016). *Miocene-Pliocene strike-slip basin development along the Denali fault system in the Eastern Alaska Range: Chronostratigraphy and provenance of the McCallum formation and implications for displacement (Master of Science)*. West Lafayette, Indiana: Purdue Univ.

Anagnostou, E., John, E. H., Edgar, K. M., Foster, G. L., Ridgwell, A., Inglis, G. N., et al. (2016). Changing atmospheric CO2 concentration was the primary driver of early Cenozoic climate. *Nature*, *533*(7603), 380–384. https://doi.org/10.1038/nature17423

Anderson, L., Berkelhammer, M., Barron, J. A., Steinman, B. A., Finney, B. P., & Abbott, M. B. (2016). Lake oxygen isotopes as recorders of North American Rocky Mountain hydroclimate: Holocene patterns and variability at multi-decadal to millennial time scales. *Global and Planetary Change*, *137*, 131–148. https://doi.org/10.1016/j.gloplacha.2015.12.021

Anovitz, L. M., Cole, D. R., & Riciputi, L. R. (2009). Low-temperature isotopic exchange in obsidian: Implications for diffusive mechanisms. *Geochimica et Cosmochimica Acta*, *73*(13), 3795–3806. https://doi.org/10.1016/j.gca.2009.02.035

Ballantyne, A. P., Greenwood, D. R., Sinninghe Damsté, J. S., Csank, A. Z., Eberle, J. J., & Rybczynski, N. (2010). Significantly warmer Arctic surface temperatures during the Pliocene indicated by multiple independent proxies. *Geology*, *38*(7), 603–606. https://doi.org/10.1130/G30815.1

Beerling, D. J., & Royer, D. L. (2011). Convergent cenozoic CO2 history. *Nature Geoscience*, *4*(7), 418–420. https://doi.org/10.1038/ngeo1186

Benowitz, J. A., Davis, K., & Roeske, S. (2019). A river runs through it both ways across time: 40Ar/39Ar detrital and bedrock muscovite geochronology constraints on the Neogene paleodrainage history of the Nenana River system, Alaska range. *Geosphere*, *15*(3), 682–701. https://doi.org/10.1130/GES01673.1

Benowitz, J. A., Fowell, S. J., Addison, J., & Layer, P. (2007). Tectonic and paleoclimatic significance of early Pliocene palynofloras from the southeastern Alaska Range. *Geological Society of America Abstracts with Programs*, *39*(4), 53.

Benowitz, J. A., Layer, P. W., Armstrong, P., Perry, S. E., Haeussler, P. J., Fitzgerald, P. G., & VanLaningham, S. (2011). Spatial variations in focused exhumation along a continental-scale strike-slip fault: The Denali fault of the eastern Alaska Range. *Geosphere*, *7*(2), 455–467. https://doi.org/10.1130/GES00589.1

Benowitz, J. A., Layer, P. W., & Vanlaningham, S. (2014). Persistent long-term (c. 24 Ma) exhumation in the Eastern Alaska Range constrained by stacked thermochronology. *Advances in 40Ar/39Ar Dating: From Archaeology to Planetary Sciences*, *378*(1), 225–243.

Berkelhammer, S. E., Brueseke, M. E., Benowitz, J. A., Trop, J. M., Davis, K., Layer, P. W., & Weber, M. (2019). Geochemical and geochronological records of tectonic changes along a flat-slab arc-transform junction: Circa 30 Ma to ca. 19 Ma Sonya Creek volcanic field, Wrangell Arc, Alaska. *Geosphere*, *15*(5), 1508–1538. https://doi.org/10.1130/GES02114.1

Berner, J., Symon, C., Arris, L., Heal, O. W., Arctic Climate Impact Assessment, National Science Foundation (U.S.), & United States (2005). *Arctic climate impact assessment*. Cambridge; New York, N.Y: Cambridge University Press.

Bill, N. S., Mix, H. T., Clark, P. U., Reilly, S. P., Jensen, B. J. L., & Benowitz, J. A. (2018). A stable isotope record of late Cenozoic surface uplift of southern Alaska. *Earth and Planetary Science Letters*, *482*, 300–311. https://doi.org/10.1016/j.epsl.2017.11.029

Bindeman, I. N., & Lowenstern, J. B. (2016). Low-δD hydration rinds in Yellowstone perlites record rapid syneruptive hydration during glacial and interglacial conditions. *Contributions to Mineralogy and Petrology*, *171*(11), 1–24. https://doi.org/10.1007/s00410-016-1293-1

Bowen, G. J., & Revenaugh, J. (2003). Interpolating the isotopic composition of modern meteoric precipitation. *Water Resources Research*, *39*(10). https://doi.org/10.1029/2003WR002086

Brueseke, M. E., Benowitz, J. A., Trop, J. M., Davis, K. N., Berkelhammer, S. E., Layer, P. W., & Morter, B. K. (2019). The Alaska Wrangell Arc: 30 Ma of subduction-related magmatism along a still active arc-transform junction. *Terra Nova*, *31*(1), 59–66. https://doi.org/10.1111/ter.12369

Burn, C. R. (1990). Implications for palaeoenvironmental reconstruction of recent ice-wedge development at Mayo, Yukon territory. *Permafrost and Periglacial Processes*, *1*(1), 3–14. https://doi.org/10.1002/ppp.3430010103

Canavan, R. R., Carrapa, B., Clementz, M. T., Quade, J., DeCelles, P. G., & Schoenbohm, L. M. (2014). Early Cenozoic uplift of the Puna Plateau, Central Andes, based on stable isotope paleoaltimetry of hydrated volcanic glass. *Geology*, *42*(5), 447–450. https://doi.org/10.1130/G35239.1

Cassel, E. J., & Breecker, D. O. (2017). Long-term stability of hydrogen isotope ratios in hydrated volcanic glass. *Geochimica et Cosmochimica Acta*, *200*, 67–86. https://doi.org/10.1016/j.gca.2016.12.001

Cassel, E. J., Breecker, D. O., Henry, C. D., Larson, T. E., & Stockli, D. F. (2014). Profile of a paleo-orogen: High topography across the present-day Basin and Range from 40 to 23 Ma. *Geology*, *42*(11), 1007–1010. https://doi.org/10.1130/G35924.1

Cassel, E. J., Graham, S. A., & Chamberlain, C. P. (2009). Cenozoic tectonic and topographic evolution of the northern Sierra Nevada, California, through stable isotope paleoaltimetry in volcanic glass. *Geology*, *37*(6), 547–550. https://doi.org/10.1130/G25572A.1

Cassel, E. J., Smith, M. E., & Jicha, B. R. (2018). The impact of slab rollback on Earth's surface: Uplift and extension in the hinterland of the North American Cordillera. *Geophysical Research Letters*, *200*, 67–86. https://doi.org/10.1029/2018GL079887

Cerling, T. E., Brown, F. H., & Bowman, J. R. (1985). Low-temperature alteration of volcanic glass: hydration, Na, K, 18O and Ar mobility. *Chemical Geology: Isotope Geoscience Section*, *52*(3-4), 281–293.

Colwyn, D. A., Brandon, M. T., Hren, M. T., Hourigan, J., Pacini, A., Cosgrove, M. G., et al. (2019). Growth and steady state of the Patagonian Andes. *American Journal of Science*, *319*(6), 431–472. https://doi.org/10.2475/06.2019.01

Craig, H. (1961). Isotopic variations in meteoric waters. *Science*, *133*(3465), 1702–1703. https://doi.org/10.1126/science.133.3465.1702

Csank, A. C., Patterson, W. P., Eglington, B. M., Rybczynski, N., & Basinger, J. F. (2011). Climate variability in the Early Pliocene Arctic: Annually resolved evidence from stable isotope values of sub-fossil wood, Ellesmere Island, Canada. *Palaeogeography, Palaeoclimatology, Palaeoecology*, *308*(3–4), 339–349. https://doi.org/10.1016/j.palaeo.2011.05.038

Csank, A. C., Tripati, A. K., Patterson, W. P., Eagle, R. A., Rybczynski, N., Ballantyne, A. P., & Eiler, J. M. (2011). Estimates of Arctic land surface temperatures during the early Pliocene from two novel proxies. *Earth and Planetary Science Letters*, *304*(3–4), 291–299. https://doi.org/10.1016/j.epsl.2011.02.030

Dang, X., Ding, W., Yang, H., Pancost, R. D., Naafs, B. D. A., Xue, J., et al. (2018). Different temperature dependence of the bacterial brGDGT isomers in 35 Chinese lake sediments compared to that in soils. *Organic Geochemistry*, *119*, 72–79. https://doi.org/10.1016/j.orggeochem.2018.02.008

Dansgaard, W. (1964). Stable isotopes in precipitation. *Tellus*, *16*(4), 436–468. https://doi.org/10.3402/tellusa.v16i4.8993

De Jonge, C., Hopmans, E. C., Zell, C. I., Kim, J.-H., Schouten, S., & Sinninghe Damsté, J. S. (2014). Occurrence and abundance of 6-methyl branched glycerol dialkyl glycerol tetraethers in soils: Implications for palaeoclimate reconstruction. *Geochimica et Cosmochimica Acta*, *141*, 97–112. https://doi.org/10.1016/j.gca.2014.06.013

Dee, D. P., Uppala, S. M., Simmons, A. J., Berrisford, P., Poli, P., Kobayashi, S., et al. (2011). The ERA-Interim reanalysis: Configuration and performance of the data assimilation system. *Quarterly Journal of the Royal Meteorological Society*, *137*(656), 553–597. https://doi.org/10.1002/qj.828

Delavau, C., Chun, K. P., Stadnyk, T., Birks, S. J., & Welker, J. M. (2015). North American precipitation isotope (δ18O) zones revealed in time series modeling across Canada and northern United States. *Water Resources Research*, *51*, 1284–1299. https://doi.org/10.1002/2014WR015687

Dettinger, M. P., & Quade, J. (2015). Testing the analytical protocols and calibration of volcanic glass for the reconstruction of hydrogen isotopes in paleoprecipitation. In Geological Society of America Memoirs (Vol. 212, pp. 261–276). Geological Society of America. https://doi.org/10.1130/2015.1212(14)

Donovan, J. J., Kremser, D., Fournelle, J. H., & Goemann, K. (2015). *Probe for EPMA: Acquisition, automation and analysis, version 11 (Version 11)*. Eugene, Oregon: Probe Software, Inc. https://www.probesoftware.com/

Elias, S. A. (2001). Mutual climatic range reconstructions of seasonal temperatures based on Late-Pleistocene fossil beetle assemblages in Eastern Beringia. *Quaternary Science Reviews*, *20*(1-3), 77–91. https://doi.org/10.1016/S0277-3791(00)00130-X

Elias, S. A., & Matthews, J. V. Jr. (2002). Arctic North American seasonal temperatures from the latest Miocene to the Early Pleistocene, based on mutual climatic range analysis of fossil beetle assemblages. *Canadian Journal of Earth Sciences*, *39*(6), 911–920. https://doi.org/10.1139/e01-096

England, J. (1987). Glaciation and the evolution of the Canadian high arctic landscape. *Geology*, *15*(5), 419–424. https://doi.org/10.1130/0091-7613(1987)15<419:GATEOT>2.0.CO;2

Enkelmann, E., Garver, J. I., & Pavlis, T. L. (2008). Rapid exhumation of ice-covered rocks of the Chugach–St. Elias orogen, southeast Alaska. *Geology*, *36*(12), 915–918. https://doi.org/10.1130/G2252A.1

Enkelmann, E., Piestrzeniewicz, A., Falkowski, S., Stübner, K., & Ehlers, T. A. (2017). Thermochronology in southeast Alaska and southwest Yukon: Implications for North American Plate response to terrane accretion. *Earth and Planetary Science Letters*, *457*, 348–358. https://doi.org/10.1016/j.epsl.2016.10.032

Enkelmann, E., Zeitler, P. K., Garver, J. I., Pavlis, T. L., & Hooks, B. P. (2010). The thermochronological record of tectonic and surface process interaction at the Yakutat–North American collision zone in southeast Alaska. *American Journal of Science*, *310*(4), 231–260. https://doi.org/10.2475/04.2010.01

Fan, M., Heller, P., Allen, S. D., & Hough, B. G. (2014). Middle Cenozoic uplift and concomitant drying in the central Rocky Mountains and adjacent Great Plains. *Geology*, *42*(6), 547–550. https://doi.org/10.1130/G35444.1

Feakins, S. J., Wu, M. S., Ponton, C., & Tierney, J. E. (2019). Biomarkers reveal abrupt switches in hydroclimate during the last glacial in southern California. *Earth and Planetary Science Letters*, *515*, 164–172. https://doi.org/10.1016/j.epsl.2019.03.024

Field, R. D., Moore, G. W. K., Holdsworth, G., & Schmidt, G. A. (2010). A GCM-based analysis of circulation controls on $\delta^{18}O$ in the southwest Yukon, Canada: Implications for climate reconstructions in the region. *Geophysical Research Letters*, *37*(5), L05706. https://doi.org/10.1029/2009GL041408

Fitzgerald, P. G., Stump, E., & Redfield, T. F. (1993). Late cenozoic uplift of denali and its relation to relative plate motion and fault morphology. *Science*, *259*(5094), 497–499. https://doi.org/10.1126/science.259.5094.497

Friedman, I., Gleason, J., Sheppard, R. A., & Gude, A. J. (1993). Deuterium fractionation as water diffuses into silicic volcanic ash. In Climate Change in Continental Isotopic Records (pp. 321–323). https://doi.org/10.1029/GM078p0321

Friedman, I., Gleason, J., & Warden, A. (1993). *Ancient climate from deuterium content of water in volcanic glass*, *Geophysical Monograph Series*, (pp. 309–319). Washington, D. C: American Geophysical Union. https://doi.org/10.1029/GM078p0309

Friedman, I., Gleason, J., Wilcox, R., & Warden, A. (1992). Modeling of ancient climate from deuterium content of water in volcanic glass. *Quaternary International*, *13–14*(C), 201–203. https://doi.org/10.1016/1040-6182(92)90029-2

Friedman, I., & Long, W. (1976). Hydration rate of obsidian. *Science (New York, N.Y.)*, *191*(4225), 347–352. https://doi.org/10.1126/science.191.4225.347

Friedman, I., Smith, R. L., & Long, W. D. (1966). Hydration of natural glass and formation of perlite. *GSA Bulletin*, *77*(3), 323–328. https://doi.org/10.1130/0016-7606(1966)77[323:HONGAF]2.0.CO;2

Froese, D. G., Barendregt, R. W., Enkin, R. J., & Baker, J. (2000). Paleomagnetic evidence for multiple late Pliocene-early Pleistocene glaciations in the Klondike area, Yukon territory. *Canadian Journal of Earth Sciences*, *37*(6), 863–877. https://doi.org/10.1139/e00-014

Froese, D. G., Zazula, G. D., & Reyes, A. V. (2006). Seasonality of the late Pleistocene Dawson tephra and exceptional preservation of a buried riparian surface in central Yukon Territory, Canada. *Quaternary Science Reviews*, *25*(13–14), 1542–1551. https://doi.org/10.1016/j.quascirev.2006.01.028

Froese, D. G., Zazula, G. D., Westgate, J. A., Preece, S. J., Sanborn, P. T., Reyes, A. V., & Pearce, N. J. G. (2009). The Klondike goldfields and Pleistocene environments of Beringia. *GSA Today*, *19*(8), 4. https://doi.org/10.1130/GSATG54A.1

Gin, S., Jollivet, P., Fournier, M., Angeli, F., Frugier, P., & Charpentier T. (2015). Origin and consequences of silicate glass passivation by surface layers. *Nature Communications*, *6*(1). https://doi.org/10.1038/ncomms7360

Gladenkov, A. Y., Oleinik, A. E., Marincovich, L., & Barinov, K. B. (2002). A refined age for the earliest opening of Bering Strait. *Palaeogeography, Palaeoclimatology, Palaeoecology*, *183*(3-4), 321–328. https://doi.org/10.1016/s0031-0182(02)00249-3

Hansen, J., Sato, M., Russell, G., & Kharecha, P. (2013). Climate sensitivity, sea level and atmospheric carbon dioxide. *Philosophical Transactions of the Royal Society A: Mathematical, Physical and Engineering Sciences*, *371*(2001), 31. https://doi.org/10.1098/rsta.2012.0294

Haywood, A. M., Dowsett, H. J., Dolan, A. M., Rowley, D., Abe-Ouchi, A., Otto-Bliesner, B., et al. (2016). The Pliocene Model Intercomparison Project (PlioMIP) Phase 2: Scientific objectives and experimental design. *Climate of the Past*, *12*(3), 663–675. https://doi.org/10.5194/cp-12-663-2016

Herbert, T. D., Lawrence, K. T., Tzanova, A., Peterson, L. C., Caballero-Gill, R., & Kelly, C. S. (2016). Late Miocene global cooling and the rise of modern ecosystems. *Nature Geoscience*, *9*(11), 843–847. https://doi.org/10.1038/ngeo2813

Hopmans, E. C., Schouten, S., & Sinninghe Damsté, J. S. (2016). The effect of improved chromatography on GDGT-based palaeoproxies. *Organic Geochemistry*, *93*, 1–6. https://doi.org/10.1016/j.orggeochem.2015.12.006

IAEA/WMO. (2018). Global Network of Isotopes in Precipitation. Retrieved from http://www.iaea.org/water

Jensen, B. J. L., Evans, M. E., Froese, D. G., & Kravchinsky, V. A. (2016). 150,000 years of loess accumulation in central Alaska. *Quaternary Science Reviews*, *135*, 1–23. https://doi.org/10.1016/j.quascirev.2016.01.001

Jensen, B. J. L., Froese, D. G., Preece, S. J., Westgate, J. A., & Stachel, T. (2008). An extensive middle to late Pleistocene tephrochronologic record from east-central Alaska. *Quaternary Science Reviews*, *27*(3–4), 411–427. https://doi.org/10.1016/j.quascirev.2007.10.010

Johnsen, S. J., Dahl-Jensen, D., Gundestrup, N., Steffensen, J. P., Clausen, H. B., Miller, H., Masson-Delmotte, V., Sveinbjörnsdottir, A. E., & White, J. (2001). Oxygen isotope and palaeotemperature records from six Greenland ice-core stations: Camp Century, Dye-3, GRIP, GISP2, Renland and NorthGRIP. *Journal of Quaternary Science*, *16*(4), 299–307. https://doi.org/10.1002/jqs.622

Keeling, C. D., Piper, S. C., Bacastow, R. B., Wahlen, M., Whorf, T. P., Heimann, M., & Meijer, H. A. (2001). Exchanges of atmospheric CO2 and 13CO2 with the terrestrial biosphere and oceans from 1978 to 2000. I. Global Aspects. Retrieved from https://escholarship.org/uc/item/09v319r9

Kunk, M. J. (1995). 40Ar/39Ar age-spectrum data for hornblende, plagioclase and biotite from tephras collected at Dan Creek and McCallum Creek, Alaska and in the Klondike Placer district near Dawson, Yukon Territory, Canada (USGS Numbered Series). Reston, Virginia.

Lease, R. O., Haeussler, P. J., & O'Sullivan, P. (2016). Changing exhumation patterns during Cenozoic growth and glaciation of the Alaska Range: Insights from detrital thermochronology and geochronology. *Tectonics*, *35*, 934–955. https://doi.org/10.1002/2015TC004067

Leopold, E. B., & Liu, G. (1994). A long pollen sequence of Neogene age, Alaska Range. *Quaternary International*, *22*, 103–140.

Leschik, M., Heide, G., Frischat, G. H., Behrens, H., Wiedenbeck, M., Wagner, N., et al. (2004). Determination of H2O and D2O contents in rhyolitic glasses. *European Journal of Glass Science and Technology Part B Physics and Chemistry of Glasses*, *45*, 238–251.

Martin, E., Bindeman, I., Balan, E., Palandri, J., Seligman, A., & Villemant, B. (2017). Hydrogen isotope determination by TC/EA technique in application to volcanic glass as a window into secondary hydration. *Journal of Volcanology and Geothermal Research*, *348*, 49–61. https://doi.org/10.1016/j.jvolgeores.2017.10.013

Matthews, J. V., Westgate, J. A., Ovenden, L., Carter, L. D., & Fouch, T. (2003). Stratigraphy, fossils, and age of sediments at the upper pit of the l=Lost Chicken gold mine: New information on the late Pliocene environment of east central Alaska. *Quaternary Research*, *60*(1), 9–18. https://doi.org/10.1016/S0033-5894(03)00087-5

Mix, H. T., & Chamberlain, C. P. (2014). Stable isotope records of hydrologic change and paleotemperature from smectite in Cenozoic western North America. *Geochimica et Cosmochimica Acta*, *141*, 532–546. https://doi.org/10.1016/j.gca.2014.07.008

Mock, C. J., Bartlein, P. J., & Anderson, P. M. (1998). Atmospheric circulation patterns and spatial climatic variations in Beringia. *International Journal of Climatology*, *18*(10), 1085–1104. https://doi.org/10.1002/(SICI)1097-0088(199808)18:10<1085::AID-JOC305>3.0.CO;2-K

Muhs, D., Pigati, S., Budahn, J. L., Skipp, G., Bettis, A., & Jensen, B. (2018). Origin of last-glacial loess in the western Yukon-Tanana Upland, central Alaska, USA. *Quaternary Research*, *89*(3), 797–819. https://doi.org/10.1017/qua.2018.11

Mulch, A., Sarna-Wojcicki, A. M., Perkins, M. E., & Chamberlain, C. P. (2008). A Miocene to Pleistocene climate and elevation record of the Sierra Nevada (California). *Proceedings of the National Academy of Sciences*, *105*(19), 6819–6824. https://doi.org/10.1073/pnas.0708811105

Naafs, B. D. A., Gallego-Sala, A. V., Inglis, G. N., & Pancost, R. D. (2017). Refining the global branched glycerol dialkyl glycerol tetraether (brGDGT) soil temperature calibration. *Organic Geochemistry*, *106*, 48–56. https://doi.org/10.1016/j.orggeochem.2017.01.009

Parruzot, B., Jollivet, P., Rébiscoul, D., & Gin, S. (2015). Long-term alteration of basaltic glass: Mechanisms and rates. *Geochimica et Cosmochimica Acta*, *154*, 28–48. https://doi.org/10.1016/j.gca.2014.12.011

Pingel, H., Alonso, R. N., Mulch, A., Rohrmann, A., Sudo, M., & Strecker, M. R. (2014). Pliocene orographic barrier uplift in the southern Central Andes. *Geology*, *42*(8), 691–694. https://doi.org/10.1130/G35538.1

Pingel, H., Strecker, M. R., Mulch, A., Alonso, R. N., Cottle, J., & Rohrmann, A. (2020). Late Cenozoic topographic evolution of the Eastern Cordillera and Puna Plateau margin in the southern Central Andes (NW Argentina). *Earth and Planetary Science Letters*, *535*, 116112. https://doi.org/10.1016/j.epsl.2020.116112

Poage, M. A., & Chamberlain, C. P. (2001). Empirical relationships between elevation and the stable isotope composition of precipitation and surface waters: Considerations for studies of paleoelevation change. *American Journal of Science*, *301*(1), 1–15. https://doi.org/10.2475/ajs.301.1.1

Porter, T. J., Froese, D. G., Feakins, S. J., Bindeman, I. N., Mahony, M. E., Pautler, B. G., et al. (2016). Multiple water isotope proxy reconstruction of extremely low last glacial temperatures in Eastern Beringia (Western Arctic). *Quaternary Science Reviews*, *137*, 113–125. https://doi.org/10.1016/j.quascirev.2016.02.006

Porter, T. J., Schoenemann, S. W., Davies, L. J., Steig, E. J., Bandara, S., & Froese, D. G. (2019). Recent summer warming in northwestern Canada exceeds the Holocene thermal maximum. *Nature Communications*, *10*(1), 1631. https://doi.org/10.1038/s41467-019-09622-y

Pound, M. J., Lowther, R. I., Peakall, J., Chapman, R. J., & Salzmann, U. (2015). Palynological evidence for a warmer boreal climate in the Late Pliocene of the Yukon Territory, Canada. *Palynology*, *39*(1), 91–102. https://doi.org/10.1080/01916122.2014.940471

Preece, S. J., Westgate, J. A., Froese, D. G., Pearce, N. J. G., Perkins, W. T., & Fisher, T. (2011). A catalogue of late Cenozoic tephra beds in the Klondike goldfields and adjacent areas, Yukon Territory. *Canadian Journal of Earth Sciences*, *48*(10), 1386–1418. https://doi.org/10.1139/e10-110

Qi, H., Coplen, T. B., Gehre, M., Vennemann, T. W., Brand, W. A., Geilmann, H., et al. (2017). New biotite and muscovite isotopic reference materials, USGS57 and USGS58, for δ2H measurements—A replacement for NBS 30. *Chemical Geology*, *467*, 89–99. https://doi.org/10.1016/j.chemgeo.2017.07.027

Quade, J., Garzione, C., & Eiler, J. M. (2007). Paleoelevation reconstruction using pedogenic carbonates. *Reviews in Mineralogy and Geochemistry*, *66*(1), 53–87. https://doi.org/10.2138/rmg.2007.66.3

Reyes, A. V., Froese, D. G., & Jensen, B. J. L. (2010). Permafrost response to last interglacial warming: Field evidence from non-glaciated Yukon and Alaska. *Quaternary Science Reviews*, *29*(23–24), 3256–3274. https://doi.org/10.1016/j.quascirev.2010.07.013

Rohling, E. J., Foster, G. L., Grant, K. M., Marino, G., Roberts, A. P., Tamisiea, M. E., & Williams, F. (2014). Sea-level and deep-sea-temperature variability over the past 5.3 million years. *Nature*, *508*(7497), 477–482. https://doi.org/10.1038/nature13230

Russell, J. M., Hopmans, E. C., Loomis, S. E., Liang, J., & Sinninghe Damsté, J. S. (2018). Distributions of 5- and 6-methyl branched glycerol dialkyl glycerol tetraethers (brGDGTs) in East African lake sediment: Effects of temperature, pH, and new lacustrine paleotemperature calibrations. *Organic Geochemistry*, *117*, 56–69. https://doi.org/10.1016/j.orggeochem.2017.12.003

Schrag, D. P., Adkins, J. F., McIntyre, K., Alexander, J. L., Hodell, D. A., Charles, C. D., & McManus, J. F. (2002). The oxygen isotopic composition of seawater during the Last Glacial Maximum. *Quaternary Science Reviews*, *21*(1-3), 331–342. https://doi.org/10.1016/S0277-3791(01)00110-X

Seligman, A. N., Bindeman, I. N., Watkins, J. M., & Ross, A. M. (2016). Water in volcanic glass: From volcanic degassing to secondary hydration. *Geochimica et Cosmochimica Acta*, *191*, 216–238. https://doi.org/10.1016/j.gca.2016.07.010

Serreze, M. C., & Barry, R. G. (2011). Processes and impacts of Arctic amplification: A research synthesis. *Global and Planetary Change*, *77*(1–2), 85–96. https://doi.org/10.1016/j.gloplacha.2011.03.004

Sortor, R. N., Goehring, B. M., Bemis, S. P., Ruleman, C., Nichols, K. A., Ward, D. J., & Frothingham, M. (2017). Determining timing of Alaska Range exhumation and glaciation through cosmogenic nuclide burial dating. AGU Fall Meeting Abstracts, 21. Retrieved from http://adsabs.harvard.edu/abs/2017AGUFMEP21A1820S

Stenni, B., Buiron, D., Frezzotti, M., Albani, S., Barbante, C., Bard, E., et al. (2011). Expression of the bipolar see-saw in Antarctic climate records during the last deglaciation. *Nature Geoscience*, *4*(1), 46–49. https://doi.org/10.1038/ngeo1026

Taylor, B. E., Eichelberger, J. C., & Westrich, H. R. (1983). Hydrogen isotopic evidence of rhyolitic magma degassing during shallow intrusion and eruption. *Nature*, *306*(5943), 541–545. https://doi.org/10.1038/306541a0

Thomas, E. K., Castañeda, I. S., McKay, N. P., Briner, J. P., Salacup, J. M., Nguyen, K. Q., & Schweinsberg, A. D. (2018). A wetter Arctic coincident with hemispheric warming 8,000 years ago. *Geophysical Research Letters*, *45*(19), 10,637–10,647. https://doi.org/10.1029/2018GL079517

Tierney, J. E. (2012). GDGT thermometry: Lipid tools for reconstructing paleotemperatures. *The Paleontological Society Papers*, *18*, 115–132. https://doi.org/10.1017/S1089332600002588

Triplehorn, D. M. (1976). Clay mineralogy and petrology of the coal-bearing group near Healy (No. GR 52). Alaska Division of Geological & Geophysical Surveys. https://doi.org/10.14509/388

Triplehorn, D. M., Drake, J., & Layer, P. W. (1999). Preliminary 40Ar/39Ar ages from two units in the Usibelli Group, Healy, Alaska: New light on some old problems: Alaska Division of Geological and Geophysical Surveys, Short Notes on Alaskan Geology (Vol. 119).

Trop, J. M., Benowitz, J., Cole, R. B., & O'Sullivan, P. (2019). Cretaceous to Miocene magmatism, sedimentation, and exhumation within the Alaska Range suture zone: A polyphase reactivated terrane boundary. *Geosphere*, *15*(4), 1066–1101. https://doi.org/10.1130/GES02014.1

Viau, A. E., Gajewski, K., Sawada, M. C., & Bunbury, J. (2008). Low- and high-frequency climate variability in eastern Beringia during the past 25 000 years. *Canadian Journal of Earth Sciences*, *45*(11), 1435–1453. https://doi.org/10.1139/E08-036

Wahrhaftig, B. C., Wolfe, J. A., Leopold, E. B., & Lanphere, M. A. (1969). The coal-bearing group in the Nenana coal field, Alaska. *Contributions to Stratigraphy*, *1274*(D).

Waldien, T. S., Roeske, S. M., Benowitz, J. A., Allen, W. K., Ridgway, K. D., & O'Sullivan, P. B. (2018). Late Miocene to Quaternary evolution of the McCallum Creek thrust system, Alaska: Insights for range-boundary thrusts in transpressional orogens. *Geosphere*, *14*(6), 2379–2406. https://doi.org/10.1130/GES01676.1

Westgate, J. A., Preece, S. J., Froese, D. G., Telka, A. M., Storer, J. E., Pearce, N. J. G., et al. (2009). Gold Run tephra: A middle Pleistocene stratigraphic and paleoenvironmental marker across west-Central Yukon territory, Canada. *Canadian Journal of Earth Sciences*, *46*(6), 465–478. https://doi.org/10.1139/E09-029

Westgate, J. A., Sandhu, A. S., & Preece, S. J. (2002). Age of the gold-bearing White Channel Gravel, Klondike district, Yukon. *Yukon Exploration and Geology*, *2002*, 241–250.

Westgate, J. A., Stemper, B. A., & Péwé, T. L. (1990). A 3 my record of Pliocene-Pleistocene loess in, interior Alaska. *Geology*, *18*(9), 858–861. https://doi.org/10.1130/0091-7613(1990)018<0858:AMYROP>2.3.CO;2

White, J. M., Ager, T. A., Adam, D. P., Leopold, E. B., Liu, G., Jette, H., & Schweger, C. E. (1997). An 18 million year record of vegetation and climate change in northwestern Canada and Alaska: Tectonic and global climatic correlates. *Palaeogeography, Palaeoclimatology, Palaeoecology*, *130*(1–4), 293–306. https://doi.org/10.1016/S0031-0182(96)00146-0

Wolfe, J. A. (1994). An analysis of Neogene climates in Beringia. *Palaeogeography, Palaeoclimatology, Palaeoecology*, *108*(3-4), 207–216. https://doi.org/10.1016/0031-0182(94)90234-8

Zachos, J., Pagani, M., Sloan, L., Thomas, E., & Billups, K. (2001). Trends, rhythms, and aberrations in global climate 65 Ma to present. *Science*, *292*, 8.

Zazula, G. D., Froese, D. G., Schweger, C. E., Mathewes, R. W., Beaudoin, A. B., Telka, A. M., et al. (2003). Palaeobotany: Ice-age steppe vegetation in east Beringia. *Nature*, *423*(6940), 603. https://doi.org/10.1038/423603a

Zellers, S. D. (1995). Foraminiferal sequence biostratigraphy and seismic stratigraphy of a tectonically active margin; the Yakataga Formation, northeastern Gulf of Alaska. *Marine Micropaleontology*, *26*(1-4), 255–271. https://doi.org/10.1016/0377-8398(95)00031-3